Proceedings of the ASME 2015 International Mechanical Engineering Congress & Exposition
IMECE2015
November 13-19, 2015, Houston, Texas, USA

IMECE2015-52696

VIRTUAL SIMULATION OF THE EFFECTS OF INTRACRANIAL FLUID CAVITATION IN BLAST-INDUCED TRAUMATIC BRAIN INJURY

Shivonne Haniff
Sandia National Laboratories
Albuquerque, NM 87185
shaniff@sandia.gov

Paul Taylor
Sandia National Laboratories
Albuquerque, NM 87185

Aaron Brundage
Sandia National Laboratories
Albuquerque, NM 87185

Damon Burnett
Sandia National Laboratories
Albuquerque, NM 87185

Candice Cooper
Sandia National Laboratories
Albuquerque, NM 87185

Arne Gullerud
Sandia National Laboratories
Albuquerque, NM 87185

Ryan Terpsma
Sandia National Laboratories
Albuquerque, NM 87185

ABSTRACT

A microscale model of the brain was developed in order to understand the details of intracranial fluid cavitation and the damage mechanisms associated with cavitation bubble collapse due to blast-induced traumatic brain injury (TBI). Our macroscale model predicted cavitation in regions of high concentration of cerebrospinal fluid (CSF) and blood. The results from this macroscale simulation directed the development of the microscale model of the superior sagittal sinus (SSS) region. The microscale model includes layers of scalp, skull, dura, superior sagittal sinus, falx, arachnoid, subarachnoid spacing, pia, and gray matter. We conducted numerical simulations to understand the effects of a blast load applied to the scalp with the pressure wave propagating through the layers and eventually causing the cavitation bubbles to collapse. Collapse of these bubbles creates spikes in pressure and von Mises stress downstream from the bubble locations. We investigate the influence of cavitation bubble size, compressive wave amplitude, and internal bubble pressure. The results indicate that these factors may contribute to a greater downstream pressure and von Mises stress which could lead to significant tissue damage.

Keywords: TBI, microscale model, cavitation, virtual simulation, Tillotson-Brundage Equation-of-State

INTRODUCTION

About 1.7 million people suffer from traumatic brain injury each year in the US [1]. This injury is caused by an impact, car collision, sports-related injury, violent assault or, in the case of the warfighter, ballistic projectile impact or blast exposure leading to behind-helmet brain injury. It is conjectured that one possible mechanism of brain tissue injury is intracranial cavitation caused by moderate strain rate impulsive loading to the head. This phenomenon has not been observed directly but can be inferred through a virtual simulation approach. As such, we have begun a modeling and simulation investigation of this phenomenon on both a macro- and microscale.

Our macroscale simulations employ the Sandia Human Head-Neck Model comprised of distinct models for the white matter, gray matter, falx, tentorium, ventricles, cerebrospinal fluid, skull with air-filled sinus cavities, and musculature with scalp. To simulate blast exposure of our head-neck model, we employ the Sandia Eulerian wave physics code CTH [2] which uses a finite volume method. Since fluid cavitation entails a phase transformation between the liquid and vapor phases, the capture of this phenomenon requires a special fluid model. As a result, we have employed the Tillotson-Brundage Equation-of-State model [3], to represent the volumetric response and cavitation behavior of CSF and blood. Using these tools, we have

simulated various blast exposure scenarios for blasts ranging between 2-3 atmospheres (200-300 kPa) overpressure, striking the head from the front, side, and rear directions. In all cases, our macroscale simulations predict the occurrence of cavitation with the preponderance of the phenomenon occurring where the CSF and blood concentrations were the highest.

Guided by our macroscale studies, we have initiated microscale investigations into the details of cavitation bubble collapse as it could lead to tissue injury on a sub-millimeter scale. Our microscale simulations assume the existence of cavitation bubbles, a priori, and, from that point, we investigate the tissue damaging mechanisms caused by bubble collapse and the ensuing formation of localized shock waves and hydrodynamic microjetting. In our opinion, this localized phenomenon has the potential to cause cell membrane perforation and/or cytoskeletal disruption of axonal structures.

In this paper, we will briefly present the results of our macroscale simulations that predict the existence and locations of intracranial fluid cavitation as a result of blast loading to the head. Next, we present the results of our first microscale investigation of fluid cavitation that centers on a region of superior sagittal sinus, predicted to experience cavitation of the CSF in our macroscale simulations. In particular, we will investigate the influence of cavitation bubble size and internal bubble pressure on the formation and potential tissue destructive power of the microjet that is created from bubble collapse as a result of intracranial compressive wave loading. Lastly, we will discuss future microscale modeling activities that focus on the investigation of cavitation within white matter axonal fiber bundle tracks that may lead to damage of the axons within the fiber bundles.

MACROSCALE MODELING

Our macroscale simulations employ a comprehensive head model consisting of bone (skull and cervical vertebrae), white and gray brain matter, falx and tentorium membranes (separating cerebrum hemispheres and cerebellum from cerebrum), scalp and muscle tissue, the cerebrospinal fluid (CSF), and air residing within the sinus spacing and surrounding the head-neck model. The bone is modeled by a compressible linear elastic, perfectly plastic model with an associated strain-to-failure fracture model. The white and gray matter are represented by distinct viscoelastic models. The falx and tentorium membranes and skin/muscle are represented by distinct compressible elastic models. The blast simulations are conducted using the Eulerian wave physics code CTH. The reader interested in further details of the models and the simulation methodology employed in our macroscale analyses is referred to an earlier paper by Taylor et al. [4].

In our macroscale analyses, we conducted blast exposure simulations in which blast waves were directed at the head-neck model from the front, right side, and rear directions, respectively. In each case, the blast wave exhibited the classic Friedlander blast structure [5], exhibiting an amplitude of 360 kPa (260 kPa overpressure) and a pulsewidth of 1-2 milliseconds.

In all three blast scenarios, frontal, side, and rear, our simulations predicted cavitation occurring in areas with high concentrations of CSF. Specifically, cavitation was predicted in regions surrounding and including the superior sagittal sinus as shown in Figure 1.

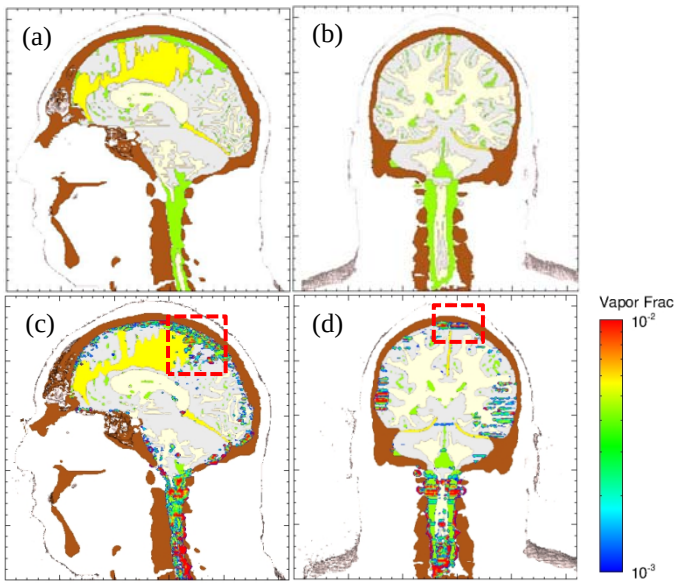

Figure 1: Macroscale simulation results predicting cavitation in Superior Sagittal Sinus from blast loading. (a) and (b): initial state showing mid-sagittal and coronal views. (c) and (d): vapor volume fraction from cavitation. Note boxed regions in (c) and (d) surrounding the superior sagittal sinus identifying presence of vapor from cavitation of cerebrospinal fluid.

MICROSCALE MODEL DESCRIPTION

We are developing microscale models of various regions within the brain where our macroscale simulations predict significant levels of blast-induced fluid cavitation. As mentioned earlier, one such region centers on a section of the superior sagittal sinus, including the various membranes and structures from the crown of the skull to the underlying gray brain matter. Our microscale model representing this region consists of the scalp, skull, dura, superior sagittal sinus, falx, arachnoid, subarachnoid spacing, pia, and gray matter (see Figure 2). To investigate the effects of cavitation, bubbles of various sizes are positioned in the cerebrospinal fluid region of the superior sagittal sinus, and in the blood passing through the blood vessels located in the subarachnoid spacing.

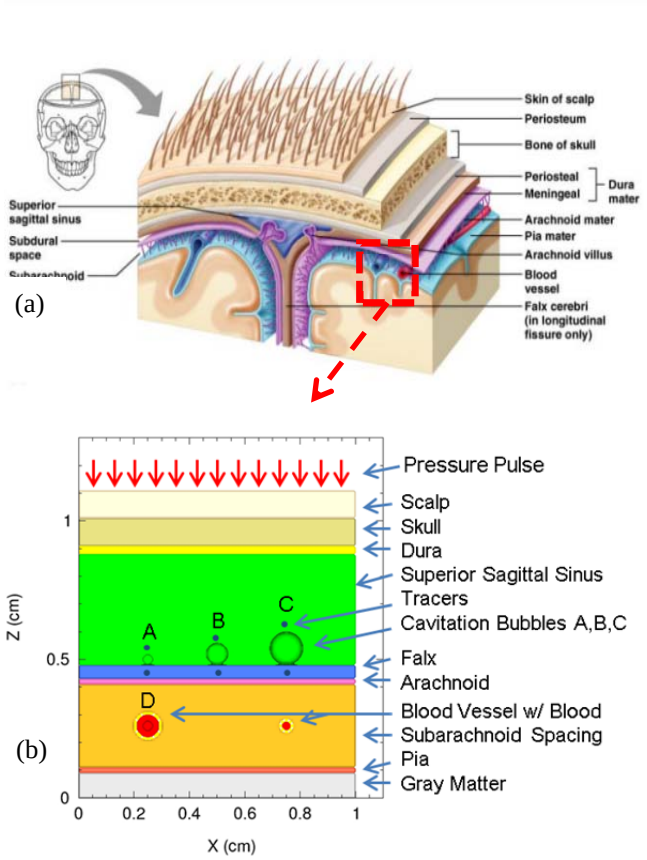

Figure 2: Microscale Model of Superior Sagittal Sinus Region. (a) Descriptive image (courtesy of [6]); (b) microscale model detail.

Equation-of-State and Constitutive Models

The volumetric and deviatoric responses of the various materials comprising the microscale model are represented by distinct equation-of-state (EOS) and constitutive models summarized in Tables I and II. Some of these models have been adapted from the constitutive models employed in the head-neck model and have been described in detail in a previous publication (e.g., bone, membranes, gray matter) [4]. An EOS describes a material's behavior as it undergoes volumetric changes, which can be either compressive or dilational. In general, an EOS is defined by the following relations:

$$P = \hat{P}(\rho, E) \quad \text{and} \quad T = \hat{T}(\rho, E), \tag{1}$$

where P is pressure, T is temperature, ρ is mass density, and E is internal energy.

To represent the constituent materials of the brain, we have drawn from the existing CTH library of EOS models. In this regard, we have assigned either a Mie-Gruneisen EOS or a Tillotson-Brundage (T-B) EOS for each material. The Mie-Gruneisen (M-G) EOS describes the volumetric response of a material experiencing thermomechanical states within some proximity to the material's shock response, as described by its shock Hugoniot curve[1]. The Mie-Gruneisen EOS works well for materials that are not expected to undergo phase transformations or significant dilational (volume increase) strains. For dilational states, the M-G EOS is linearly extrapolated to the point of failure (fracture), as specified by simulation code user.

The bone material is represented by a compressible, linear elastic perfectly plastic strength model and an accumulated strain-to-failure fracture model, fit to material properties data reported by Zhang et al. [7] and Carter [8] for cortical bone. The gray matter is considered to be a compressible, viscoelastic material and is assigned model representations similar to those proposed by Zhang et al. [7]. Specifically, this material is represented by a Mie-Gruneisen compressible equation-of-state model for the volumetric response [9] and by a separate 3-term Maxwell viscoelastic model for the deviatoric (shear) response [7]. The remaining soft tissues are represented by a Mie-Gruneisen equation-of-state (EOS) describing volumetric response and a linear elastic model describing deviatoric response. If inelastic response is anticipated, we assign a von Mises plasticity model to represent the yield strength of the material.

Blood and cerebrospinal fluid are represented by a Tillotson-Brundage equation-of-state model, which is an extension of the original Tillotson equation-of-state model [10]. The Tillotson equation-of-state model, developed in the 1960s, was originally designed to capture vaporization from compression release of metals undergoing hypervelocity impacts. While the model has been formulated for regions including compression and expansion of a material, it lacked a tensile response description that has been added to the Tillotson-Brundage version of the model.

The T-B EOS accurately captures the blood and cerebrospinal fluids' respective bulk properties under compression and their susceptibility to fluid cavitation when subjected to isotropic tension (i.e. tensile pressure) [3,11]. To our knowledge, the few finite element models that include cavitation have used properties of water [12,13]. The T-B cavitation EOS model is the first model to characterize blood and CSF using a seawater EOS and is more accurately able to capture both realistic pressure-volume response and cavitation response during shock loading. The T-B equation-of-state representation for fluids requires the assignment of a tensile (negative) pressure at which cavitation is predicted to occur. For blood and spinal fluid, we have set the cavitation pressure at -150 kPa [14] and -100 kPa [15], respectively. The T-B EOS is an extensive model and the reader is referred to reference [11] for more details about its

[1]A shock Hugoniot curve is a material property defined by a loci of shock states, over a range of shock wave amplitudes that the material can support during shock compression.

formulation and material fits. This cavitation prediction mechanism was employed in both the macroscale and microscale model.

The preexisting bubbles in the microscale model are considered to be filled with a mixture of water vapor and air (oxygen and nitrogen). Since the bubbles reside in the cerebrospinal fluid which is saturated with oxygen and nitrogen, we anticipate that when fluid cavitation occurs, the bubble contents will include not only water vapor but also a significant amount of oxygen and nitrogen, i.e., air. Since we do not necessarily have pre-existing knowledge as to the amount of water vapor and air that the cavitation (bubble-forming) process will generate, we have chosen to use internal bubble pressure as a variable in our microscale simulations. The bubble pressures chosen range from water vapor pressure of 5 kPa to atmospheric pressure of 100 kPa. As such, we have adopted a tabular equation-of-state for air to represent the internal contents of our cavitation bubbles.

Table I: Material Behavior of Microscale Model.

Material	**Volumetric Response**	**Deviatoric Response**
Scalp	Mie-Gruneisen EOS	Von Mises
Skull	Mie-Gruneisen	Von Mises
Dura	Mie-Gruneisen	Von Mises
Superior Sagittal Sinus	Tillotson-Brundage	-
Falx	Mie-Gruneisen	Von Mises
Arachnoid	Mie-Gruneisen	Von Mises
Blood Vessel	Mie-Gruneisen	Von Mises
Subarachnoid spacing	Tillotson-Brundage	-
Pia	Mie-Gruneisen	Von Mises
Gray Matter	Tillotson-Brundage	Viscoelastic
Blood	Tillotson-Brundage	-
Bubble contents	Sesame Tabular EOS	-

Table II: Material Properties of Microscale Model.

Material	**Density (g/cc)**	**Bulk Modulus (MPa)**	**Young's Modulus (MPa)**	**Poisson's Ratio**
Scalp	1.20	34.8	16.7	0.42
Skull	1.21	4762	8000	0.22
Dura	1.133	73.3	22	0.45
SSS	1.00385			
Falx	1.133	105	31.5	0.45
Arachnoid	See Pia properties			
Blood Vessel	See Dura properties			
Subarachnoid Spacing	See SSS properties			
Pia	1.133	38.33	11.5	0.45
Gray Matter	1.04	2371	-	0.49
Blood	1.05			

Simulation Methodology

Using the microscale model shown in Figure 2, we conducted numerical experiments investigating the influence of cavitation bubble size, internal bubble pressure, and compressive wave amplitude on the strength of the hydrodynamic microjet formed as a result of bubble collapse. It is difficult to perform mechanical testing at such small scales, and thus a validation of this model is unattainable at the current time given the technological limitations. Hence, we have performed parameter studies on these unknown variables.

We generated the compressive wave by imposing a boundary pressure pulse applied to the scalp at the upper boundary, attempting to mimic the blast pressure of the macroscale model calculations for the microscale model. The pressure wave propagates through the various layers of the model, reflecting and transmitting across material boundaries and inducing collapse of the bubbles placed in various locations in the superior sagittal sinus region. As a compressive wave encounters a stationary bubble, it causes the formation of a hydrodynamic jet directed downstream of the bubble. We refer to this phenomenon as microjetting. To assess the strength of each microjet as it forms downstream from each bubble, we measure both the pressure and von Mises stress in the falx. The strength of the pressure wave as it propagates through the skull is designed to vary from peak pressures of 400 to 700 kPa, reflecting the range of pressures predicted to occur in the crown of the skull as a result of blast exposure in our macroscale simulations.

In order to assure that the numerical approximation did not influence the results of our microscale simulations, a mesh convergence study was conducted. The result of this study showed that a mesh cell size of 0.025 mm was appropriate for our microscale model of the superior sagittal sinus region measuring 1 cm x 0.5 cm x 1.25 cm.

RESULTS AND DISCUSSION

The microscale model is subjected to a pressure load applied to the scalp with the preexisting cavitation bubbles of varying sizes: bubbles A, B and C with diameters of 0.04, 0.08, and 0.12 cm, respectively. Within the subarachnoid spacing is a bubble D of diameter 0.04 cm placed in the larger blood vessel. We investigated the influence of the compressive wave amplitudes from 400, 600, and 700 kPa along with various internal bubble pressures ranging from 0 to 100 kPa. As the stress wave propagates through the layers, the three bubbles collapse and produce a microjet. This microjetting event can be observed by monitoring the difference between the upstream pressures in the SSS compared to the downstream pressures in the falx.

The simulation results demonstrate the collapse of the cavitation bubbles. Note that bubble expansion is not observed since the brain constituents are at atmospheric pressure and the bubble pressures range from at or below atmospheric pressure. Figures 3-5 show the pressure time history of the microscale model for different internal bubble pressures and compressive wave amplitudes. Notice how the local high pressure region generated from bubble collapse is greater as the bubble diameter is increased. The corresponding downstream von Mises stresses for each simulation are shown in Figures 6-8 where a spike indicates the collapse of the bubble and could lead to tissue damage. As the compressive wave amplitude increases, the spikes in the downstream von Mises stress of each bubble increases. A higher internal bubble pressure results in lower downstream von Mises stresses. The spike in the von Mises stress suggests significant shearing of tissue can occur at the downstream sites.

Figures 9-11 summarize the results of varying the bubble size, internal bubble pressure, and compressive wave amplitude. Adjacent to each bubble, the downstream pressure due to bubble collapse is greater than the upstream pressure. Bubble C has the largest difference in pressures compared to the other two bubbles which suggests a greater potential for tissue damage with larger bubbles. Figure 9 shows results from the lowest peak compressive wave amplitude of 400 kPa. As the compressive wave amplitude increases to 600 kPa (Figure 10) and 700 kPa (Figure 11), the upstream and downstream pressures increase as well. These figures reinforce the results observed in Figures 3-5 that greater pressures are generated downstream from the collapse of bubbles possessing larger diameters.

Figures 12 and 13 show the results of the collapse of a cavitation bubble in the large blood vessel within the subarachnoid spacing. Figure 12 suggests that the internal bubble pressure does not affect the blood vessel blood pressure. Figure 13 displays an increase in blood pressure within the blood vessel as the compressive wave amplitude increases.

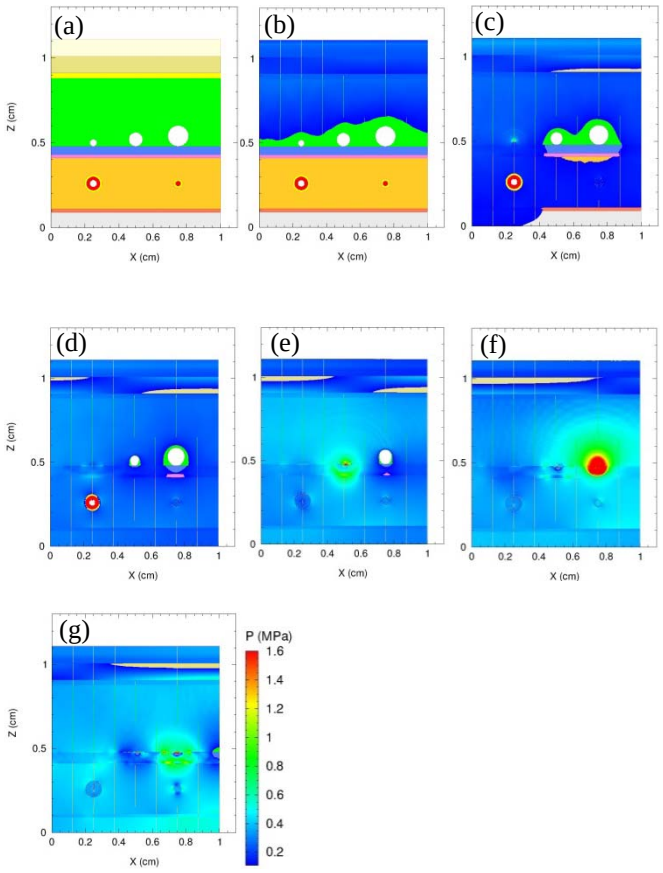

Figure 3: Pressure time history of study with 5 kPa internal bubble pressure and a 400 kPa compressive wave. (a) 0 μs (b) 10 μs (c) 20 μs (d) 30 μs (e) 40 μs (f) 50 μs (g) 60 μs. Note that the pressure scale is the same for all plots.

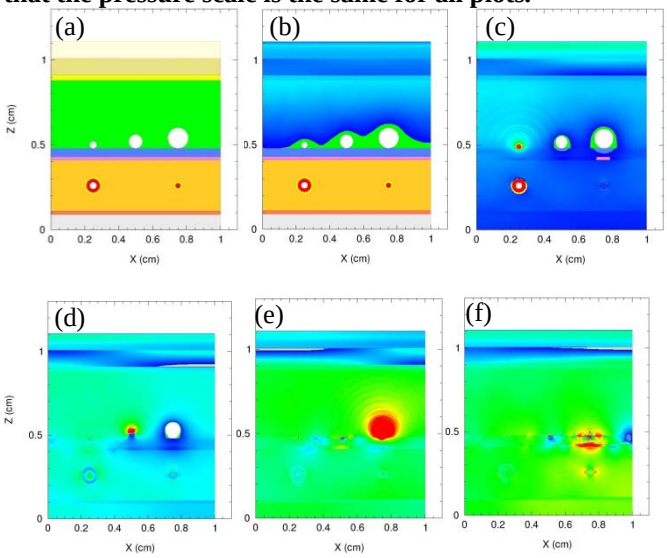

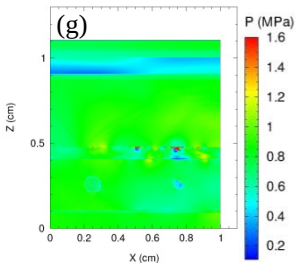

Figure 4: Pressure time history of study with 5 kPa internal bubble pressure and a 700 kPa compressive wave. (a) 0 µs (b) 10 µs (c) 20 µs (d) 30 µs (e) 40 µs (f) 50 µs (g) 60 µs. Note that the pressure scale is the same for all plots.

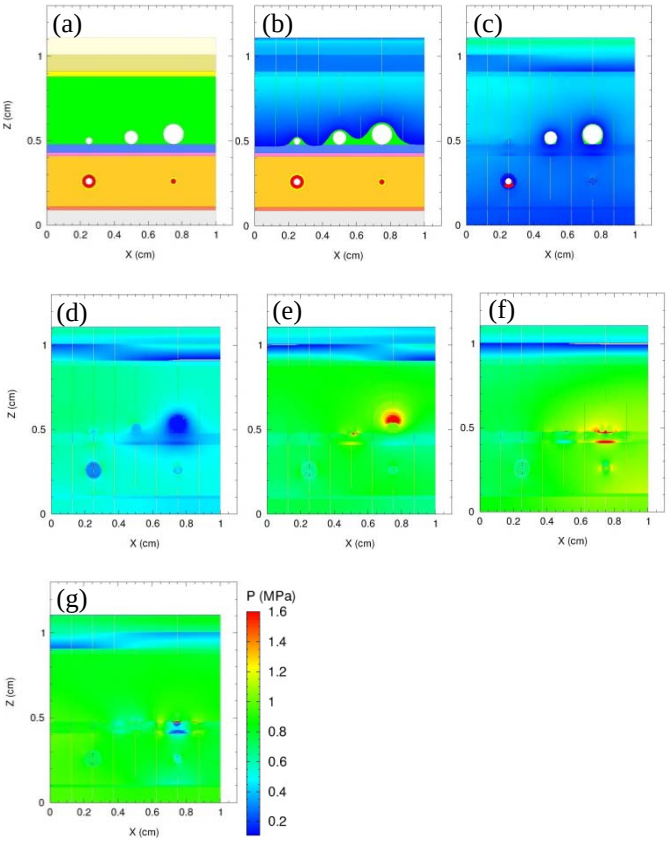

Figure 5: Pressure time history of study with 60 kPa internal bubble pressure and a 700 kPa compressive wave. (a) 0 µs (b) 10 µs (c) 20 µs (d) 30 µs (e) 40 µs (f) 50 µs (g) 60 µs. Note that the pressure scale is the same for all plots.

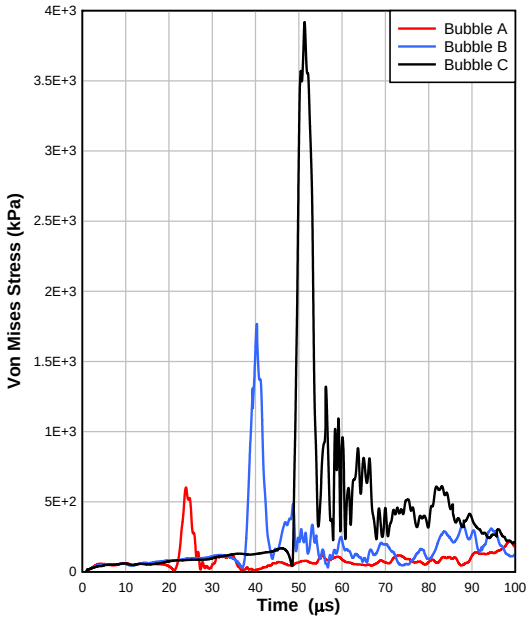

Figure 6: Downstream von Mises stress for bubbles A, B, & C with 5 kPa internal bubble pressure and a 400 kPa compressive wave.

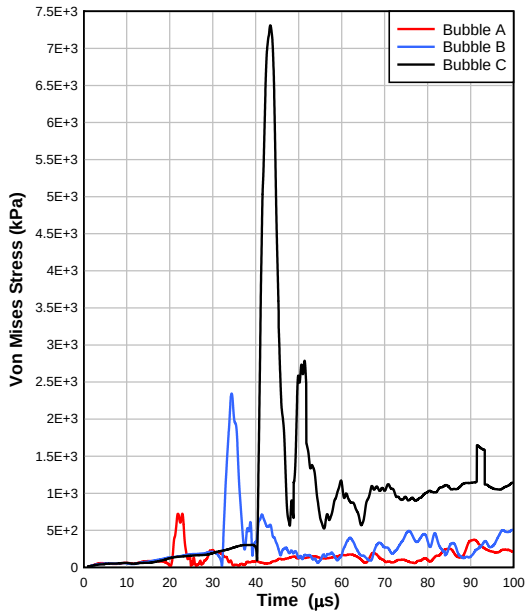

Figure 7: Downstream von Mises stress for bubbles A, B, & C with 5 kPa internal bubble pressure and a 700 kPa compressive wave.

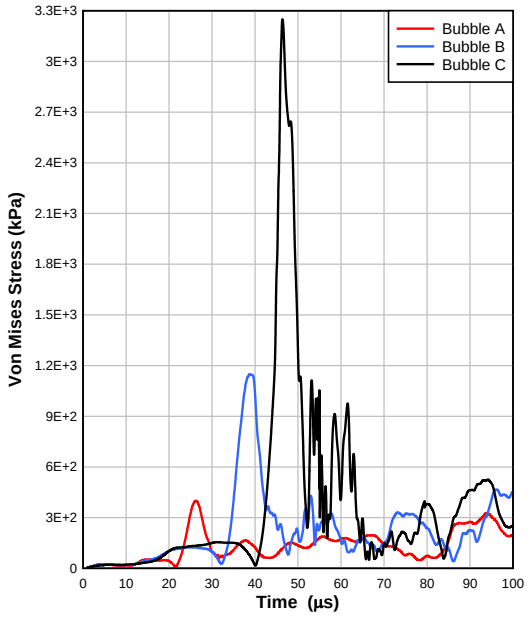

Figure 8: Downstream von Mises stress for bubbles A, B, & C with 60 kPa internal bubble pressure and a 700 kPa compressive wave.

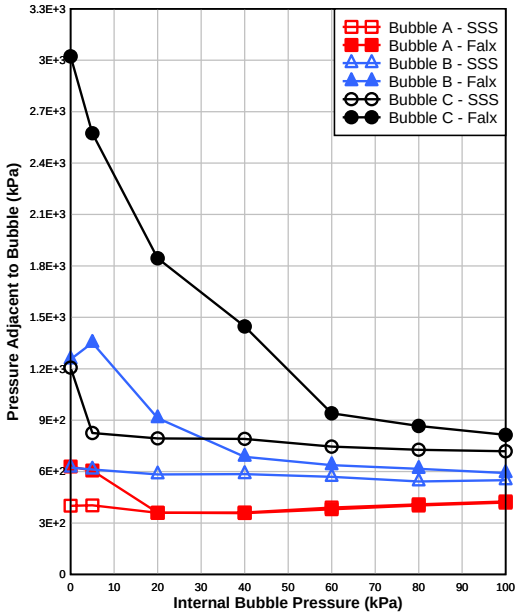

Figure 9: Pressure adjacent to bubble vs internal bubble pressure of three different bubble sizes for a 400 kPa compressive wave.

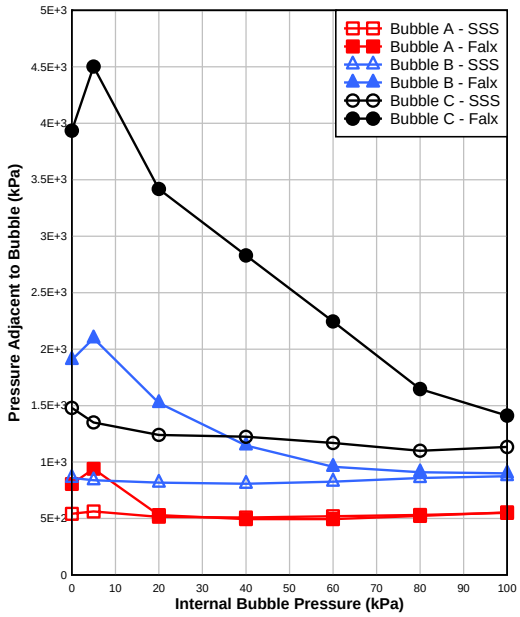

Figure 10: Pressure adjacent to bubble vs internal bubble pressure of three different bubble sizes for a 600 kPa compressive wave.

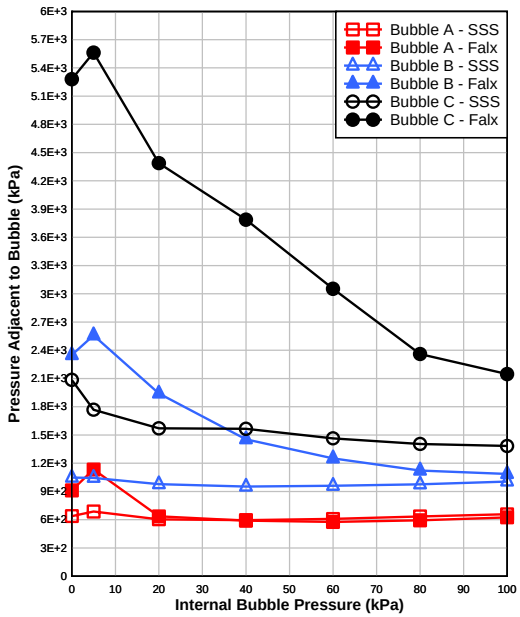

Figure 11: Pressure adjacent to bubble vs internal bubble pressure of three different bubble sizes for a 700 kPa compressive wave.

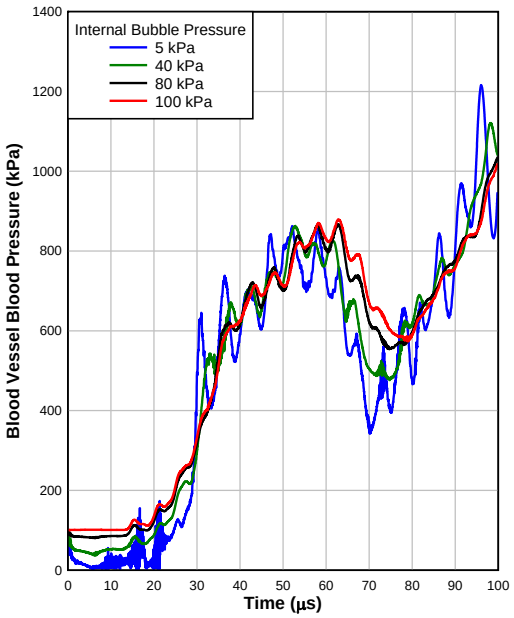

Figure 12: Blood vessel blood pressure with 700 kPa compressive wave and varying internal bubble pressure.

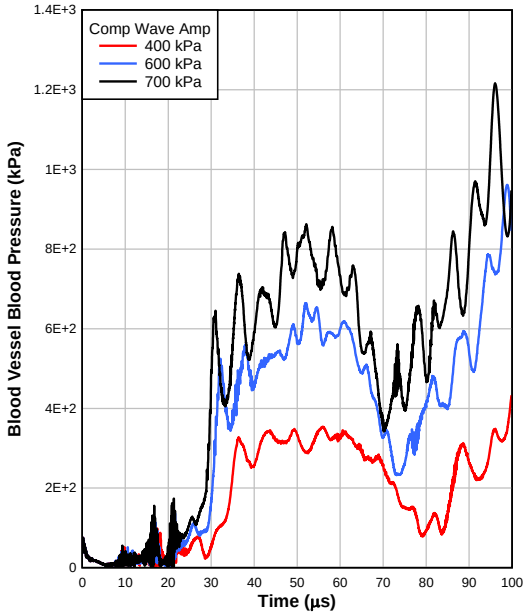

Figure 13: Blood vessel blood pressure with internal bubble pressure of 5 kPa and varying compressive wave amplitude.

Scaling relation

The results of our parametric studies on the influence of bubble size, internal pressure, and compressive wave amplitude on the strength of the microjet from bubble collapse suggest that this phenomena scales. As such, we propose the following relationship for the microjet pressure resulting from bubble collapse:

$$P_{microjet} = f(\rho, c, R, \dot{P}_{comp}), \tag{2}$$

where ρ is the bubble gas density, c is the bubble gas sound speed, R is the bubble radius, and $\dot{P}_{comp}$ is the compressive wave loading rate. Employing the Buckingham Pi-theorem of dimensional analysis [16], we can simplify eq.(2). The outcome of this exercise leads to the definitions of a critical internal bubble pressure P_{crit} and a critical bubble radius R_{crit} according to the relations

$$P_{crit} = \rho c^2, \tag{3}$$

$$R_{crit} = \frac{\rho c^3}{\dot{P}_{comp}}, \tag{4}$$

Leading to the resulting scaling relation

$$\frac{P_{microjet}}{P_{crit}} = f\left(\frac{R}{R_{crit}}\right). \tag{5}$$

A plot of all of the results from our superior sagittal sinus microscale simulations, where the compressive wave amplitude, bubble radius, and internal bubble water vapor/gas pressure are varied, is shown Figure 14. The fact that the results from all of our microscale simulations lie along the same curve confirms our suspicion that the phenomenon of cavitation bubble collapse scales relative to the critical variables P_{crit} and R_{crit}. Furthermore, P_{crit} and R_{crit} are defined in terms of quantities describing the internal conditions within the bubbles and the compressive wave loading rate.

The significance of these results lies in their support of our hypothesis that cavitation bubble collapse is most effective at damaging adjacent tissue whenever microjetting occurs as a result of the bubble collapse mechanism. The fact that this phenomenon may scale suggests that we can further investigate this damage mechanism by means of laboratory experiments that may be conducted on spatial scales not necessarily the same as those associated with cavitation-induced brain injury.

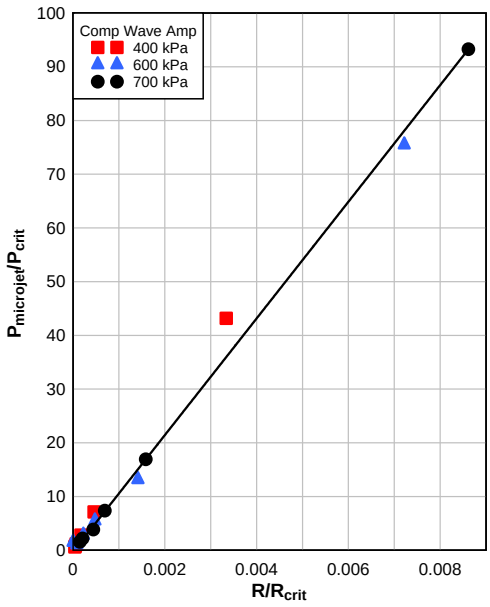

Figure 14: Scaling relation for Bubble C with varying compressive wave amplitude and internal bubble pressure.

CONCLUSION

A microscale model of the superior sagittal sinus region was developed to investigate the effects of cavitation due to factors such as intracranial wave amplitude and internal bubble pressure. A unique feature of this model is the Tillotson-Brundage model used to describe the tensile response where cavitation occurs in the fluid components of the brain. From this particular microscale study of cavitation bubble collapse within the superior sagittal sinus region, we have found that the effects of bubble collapse are dependent upon (1) the strength of the blast-induced compressive wave, (2) bubble diameter, and (3) internal bubble pressure. The effects of bubble collapse are (1) generation of a high pressure region downstream from the bubble and (2) a significant increase in von Mises (shear) stress at the downstream site. The high downstream pressure and shear stress are the result of microjetting that is observed during bubble collapse in which the upstream side of the bubble forms a jet of high velocity fluid that impact and penetrates the downstream side of the bubble.

We are also investigating this phenomenon on a finer scale, modeling white matter axonal fiber bundles and their surrounding cerebrospinal fluid environment. The details of our microscale investigations will be presented at the conference. Understanding the potential deleterious consequences of fluid cavitation in blast-induced brain injury will greatly aid in our understanding of brain injury and assist in developing mitigation strategies with which to prevent it.

ACKNOWLEDGMENTS

This work funded through the U.S. Office of Naval Research, Dr. Timothy Bentley, project funding manager, under contract number N0001414IP20020. Sandia National Laboratories is a multi-program laboratory managed and operated by Sandia Corporation, a wholly owned subsidiary of Lockheed Martin Corporation, for the United States Department of Energy's National Nuclear Security Administration under contract DE-AC04-94AL85000.

REFERENCES

[1] Centers for Disease Control and Prevention: http://www.cdc.gov/traumaticbraininjury/severe.html.

[2] Hertel, E. S., Bell, R., Elrick, M., Farnsworth, A., Kerley, G., McGlaun, J., Petney, S., Silling, S., and Taylor, P., 1993, "CTH: a software family for multi-dimensional shock physics analysis," Proc. 19th Int. Symp. Shock Waves, **1**, pp. 377–382.

[3] Brundage, A. L., 2013, "Prediction of Shock-Induced Cavitation in Water," J. Phys.: Conf. Ser. **500**, 102002.

[4] Taylor, P. A., Ludwigsen, J. S., and Ford, C. C., 2014, "Investigation of blast-induced traumatic brain injury," Brain Inj., **28**(7), pp. 879–895.

[5] Friedlander, F. G., 1947, "Simple progressive solutions of the wave equation," Math. Proc. Camb. Phil. Soc., **43**(3), pp. 360–373.

[6] Marieb, E., & Hoehn, K., 2007, *Human anatomy & physiology* (7th ed., p. 464, figure 12.24). San Francisco: Pearson Benjamin Cummings.

[7] Zhang, L., Yang, K. H., and King, A. I., 2001, "Comparison of brain responses between frontal and lateral impacts by finite element modeling," J. Neurotrauma, **18**(1), pp. 21–30.

[8] Carter, D. R., 1984, Biomechanics of bone, Appleton & Lange.

[9] Hertel, E. S., and Kerley, G. I., 1998, CTH reference manual: The equation of state package, Sandia National Laboratories, Albuquerque, NM.

[10] Tillotson J H 1962 Metallic equations of state for hypervelocity impact General Atomic Report GA-3216 (General Atomic, San Diego, CA)

[11] Brundage, A. L., 2013, "Implementation of Tillotson equation of state for hypervelocity impact of metals, geological materials, and liquids," Procedia Engr. **58**, pp.461-470.

[12] Wardlaw, A. and Goeller, J., 2010, "Cavitation as a possible traumatic brain injury (TBI) damage mechanism," IFMBE Proceedings, **32**, pp. 34-37.

[13] Panzer, M. B., Myers, B. S., Capehart, B. P., Bass, C. R., 2012, “Development of a finite element model for blast brain injury and the effects of CSF cavitation,” Ann. Biomed. Engrg. **40**(7), pp. 1530-1544.

[14] Williams, J. C., Woodward, J. F., Stonehill, m. A., Evan, A. P., McAteer, J. A., 1999, “Cell damage by lithotripter shock waves at high pressure to preclude cavitation,” Ultrasound in Med. & Biol., 25(9), 1445-1449.

[15] Brundage, A., L., 2014, personal communication.

[16] Barenblatt, G. I., 1979, *Similarity, Self-Similarity, and Intermediate Asymptotics*, Plenum Publ., New York, NY.